Journal of Materials Chemistry B

ROYAL SOCIETY OF CHEMISTRY

PAPER

View Article Online
View Journal | View Issue

Cite this: *J. Mater. Chem. B*, 2026, **14**, 2461

Co-delivery of synaptogenic and angiogenic nanoparticles in MAP scaffolds enhances post-stroke synapse formation

Nhi V. Phan,[a] Jeremy L. Thomas,[a] Aiden Pasinsky,[a] Zoe Meadows,[a] Ting Ting Li,[a] Augustus Adams,[a] Yike Zhu,[a] Anna Edgcomb,[a] Yi Shi,[a] Sihan Lyu,[a] Timothy W. Dunn[ab] and Tatiana Segura *[acd]

Received 25th September 2025,
Accepted 2nd January 2026

DOI: 10.1039/d5tb02179k

rsc.li/materials-b

Ischemic stroke remains one of the leading causes of long-term disability worldwide, depriving patients of their quality of life and physical independence. The root cause of this loss of motor movement stems from the disruption of neuronal connections in the infarct site. Limited spontaneous neural re-wiring post-stroke does provide limited functional recovery, but more than two thirds of ischemic stroke patients suffer from long-term disability for the remainder of their lives. Here, we explore the co-delivery of synaptogenic proteins with an angiogenic biomaterial to promote synapse formation in a mouse model of ischemic stroke. The angiogenic biomaterial is based on microporous annealed particle (MAP) scaffolds containing previously reported pro-angiogenic clustered vascular endothelial growth factor (CLUVENA) heparin nanoparticles. To this material, pro-synaptogenic protein thrombospondin-1 (TSP-1) was added either in soluble or clustered nanoparticle form. Co-delivery of TSP-1 with CLUVENA within MAP scaffolds led to enhanced synapse formation in and around the infarct, despite a reduction in axonal sprouting when compared to CLUVENA delivery alone. TSP-1 treatment also resulted in increased glial scar thickness and astrocytic coverage in the peri-infarct region, potentially contributing to limited axonal integration. Overall, these findings highlight the capacity of TSP-1 to modulate the synaptic and glial landscape post-stroke.

1. Introduction

Each year, millions of individuals suffer an ischemic stroke, and many are left with persistent motor and cognitive impairments resulting from the loss of neural connections within the infarcted region.[1] Healing after stroke is a dynamic but incomplete process where the timing of reparative events greatly influences functional recovery. Although limited spontaneous rewiring occurs after stroke, the molecular programs activated in the acute phase often restrict axonal sprouting and synapse formation, ultimately constraining neurological recovery in the later stages of repair.[2]

One potential therapeutic strategy is to rehabilitate the infarct space into an environment that supports neural repair. Microporous annealed particle (MAP) scaffolds are granular scaffolds made of monodispersed microgels (~100 μm in diameter) covalently annealed together to create a 3-dimensional scaffold.[3] MAP scaffolds combine the advantages of providing a substrate to encourage cellular infiltration and residency while also preventing fibrotic contraction of the infarct, thereby supporting tissue integration. Importantly, the replacement of the neurotoxic lesion with a tissue compatible biomaterial has previously been shown to reduce astrogliosis and attenuate the local microglia and macrophage response.[4] However, functional behavioral improvement in stroke models was only observed when pro-angiogenic factors such as clustered VEGF heparin nanoparticles (CLUVENA) were delivered with MAP.[5] Although this approach promoted vascularization and neurite sprouting, behavioral recovery lagged until 12 weeks, likely due to the absence of mechanisms that actively guide synaptic and engram refinement required for movement execution.

To address this gap, we sought out a bioactive molecule capable of promoting synapse formation amenable to endogenous activation. By doing so, we may mitigate the risk of excessive or maladaptive hyperconnectivity that could contribute to neuropathic pain.[6] Excitatory silent synapses are structurally mature but functionally silent, as they initially lack

[a] Department of Biomedical Engineering, Duke University, Durham NC 27708-0281, USA. E-mail: tatiana.segura@duke.edu; Tel: +1-919-660-2901
[b] Department of Neurosurgery, Duke University, Durham NC 27708-0281, USA
[c] Department of Dermatology, Duke University, Durham NC 27708-0281, USA
[d] Department of Neurology Duke University, Durham NC 27708-0281, USA

AMPA receptors necessary to generate a postsynaptic potential. However, these synapses can be unsilenced through experience-dependent plasticity, such as sensory input and learning, which aligns with the rehabilitative effects of physical therapy following stroke.[7] Notably, recent studies have shown that silent synapses are more abundant in the adult brain than previously thought, comprising approximately 30% of all excitatory synapses in the cortex.[8] One such molecule that can induce these silent synapses is thrombospondin 1 (TSP-1), which is a trimeric astrocyte-secreted glycoprotein known to promote excitatory synapse formation through its interaction with the α2δ-1 subunit of voltage-gated calcium channels on neurons.[9–11] Generally, TSP-1 is upregulated after injury in the central nervous system.[12,13] In the context of ischemic stroke, knock out of TSP-1 and -2 severely impaired axonal sprouting and synapse formation, leading to worse functional recovery despite comparable infarct size and vascular density in wild-type mice.[12] Given TSP-1's ability to generate a reservoir of synapses primed for activity-dependent refinement, we integrated this protein into a biomaterial platform as a molecular cue for post-stroke repair. Actively targeting synapse formation through a biomaterial vehicle after ischemic stroke has not yet been fully investigated. Leveraging the scaffold's spatiotemporal presentation capabilities, we aimed to guide neural circuit remodeling by supporting axonal sprouting and functional connection formation that together contribute to enhanced motor recovery.

In this work, we explore how co-delivery of a dual angiogenic and synaptogenic hydrogel MAP scaffold to the infarct site can impact tissue repair and behavioral recovery *in vivo*. By leveraging the scaffold's ability to present bioactive signals in a controlled spatiotemporal manner, we aimed to combine the vascular benefits of CLUVENA with the synaptogenic activity of TSP-1. Here, we report that co-delivery of TSP-1 (either soluble or nanoparticle-conjugated) with CLUVENA in MAP scaffolds increased synapse formation within and around the infarct site

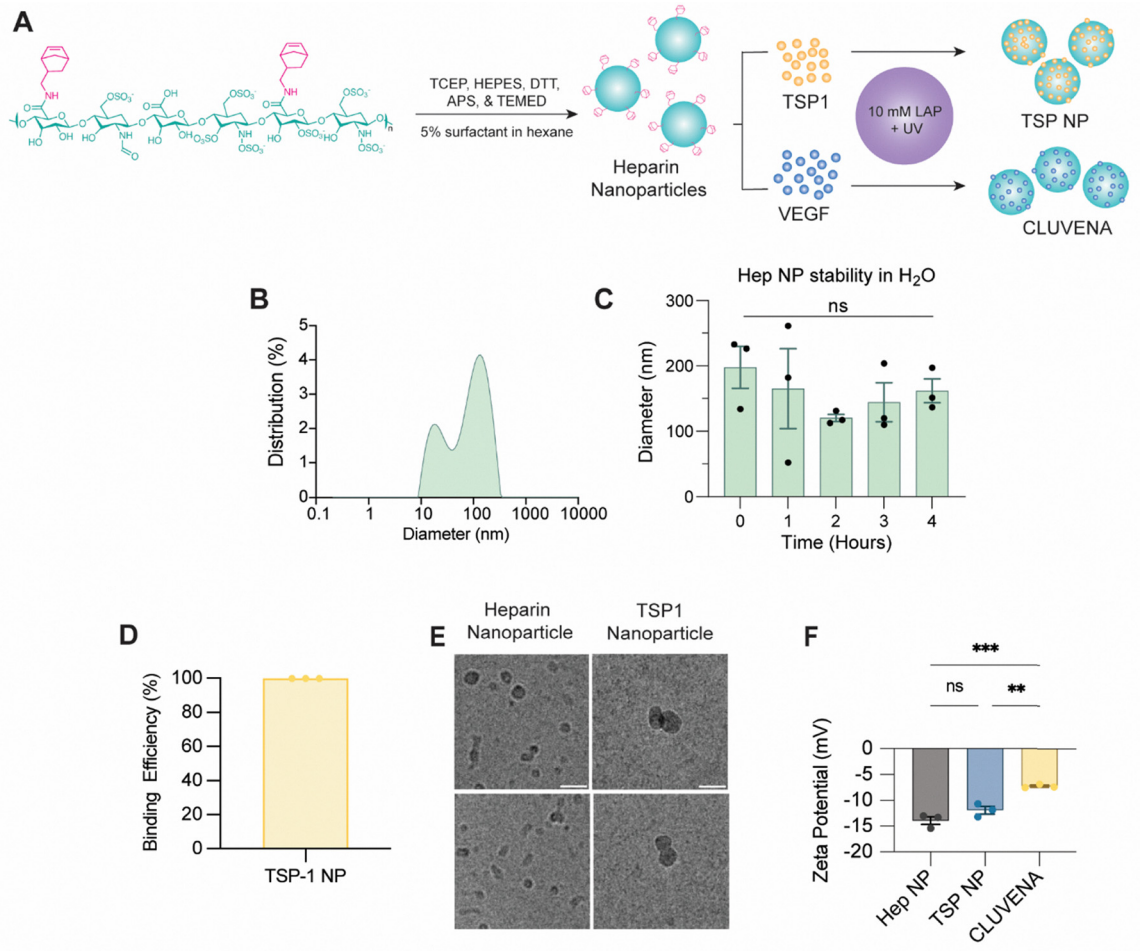

Fig. 1 Synthesis and characterization of heparin nanoparticles covalently functionalized with TSP-1. (A) Schematic depicting the method for synthesizing TSP-1 Nanoparticles (TSP NPs) and Clustered VEGF Nanoparticles (CLUVENA). (B) Dynamic light scattering data of heparin nanoparticle sizes. (C) Time-dependent aggregation behavior of heparin nanoparticles in water. $N = 3$. (D) TSP-1 binding efficiency to heparin nanoparticles as determined with a TSP-1 ELISA through the measurement of unbound TSP-1 found in the dialysate. $N = 3$. (E) CryoEM images of heparin nanoparticles and TSP NPs (F) Zeta potential measurements of heparin nanoparticles, TSP NPs, and CLUVENA, indicating the expected changes in surface charge following protein conjugation. Unadjusted p-values are indicated on the graphs and were measured using one-way ANOVA.

without disrupting angiogenesis. Although TSP-1 treatment also altered astrocytic and axonal dynamics, the overall findings establish a new therapeutic paradigm: using synaptogenesis cues embedded in biomaterials to guide neural circuit repair after ischemic stroke.

2. Results and discussion

2.1. Conjugation of TSP-1 to heparin nanoparticles enables delivery without loss of synaptogenic activity

TSP-1 has not previously been delivered as a therapeutic to promote synapse formation after stroke. Here, we explored two delivery modalities: soluble protein delivery (TSP-1 Sol) and a nanoparticle delivery approach (TSP-1 NP). For our nanoparticle formulation, we elected to use a heparin nanoparticle-based delivery system that was originally designed for VEGF delivery[5,14,15] and adapted it for TSP-1. Heparin possesses a high binding affinity for growth factors, including VEGF, FGF, and BMP, enabling it to sequester and stabilize bioactive proteins.[16–18] When formulated as a nanoparticle, heparin can not only protect its protein cargo from rapid degradation but also modulate release kinetics. We elected to use heparin nanoparticles as our delivery vehicle for TSP-1 since the TSP-1 protein itself contains a heparin-binding domain as well as free thiol groups, making it well-suited for stable conjugation *via* thiol–ene click chemistry.[19] Heparin nanoparticles were synthesized from norbornene-modified heparin, validated by NMR (Fig. S1), using an inverse emulsion polymerization method with UV initiated thiol–ene click chemistry and LAP as a radical initiator (Fig. 1A). Nanoparticles were found to be ~120 nm in diameter measured by dynamic light scattering (DLS) (Fig. 1B). To evaluate stability under biologically relevant conditions, heparin nanoparticle aggregation behavior was assessed over time in water, displaying non-significant levels of aggregation over 4 hours (Fig. 1C). We found that heparin TSP-1 bound to heparin nanoparticles with a 99.8% binding efficiency at a mass-to-mass ratio of 20 : 1 (Fig. 1D). Diameter measurements align with the cryoEM images and SEM results reported in our previous work (Fig. 1E).[5]

Surface charge analysis revealed that TSP-1 functionalization increased the zeta potential of the nanoparticles relative to naked heparin nanoparticles, while CLUVENA nanoparticles exhibited a further shift (Fig. 1F). This shift in zeta potential is expected, as covalent conjugation of proteins partially masks the highly anionic sulfate groups of heparin and introduces

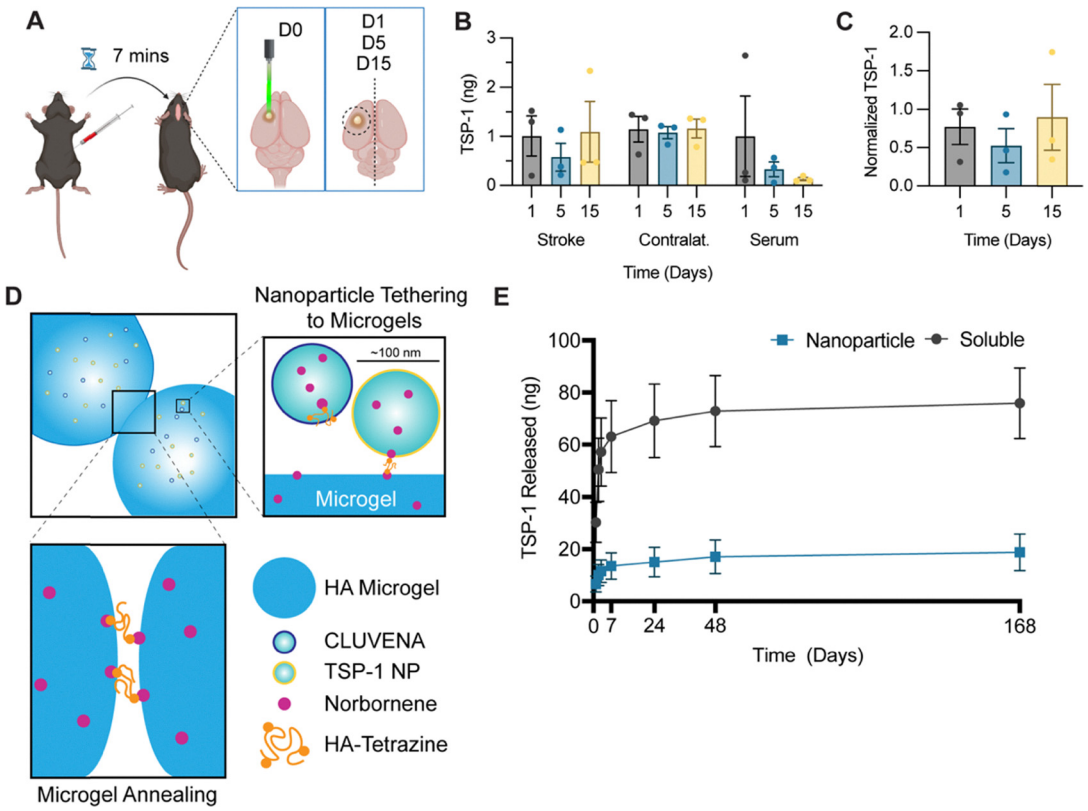

Fig. 2 Characterizing TSP-1 protein expression in a photothrombotic stroke model and sustained TSP-1 release from MAP scaffolds. (A) Experimental overview of the photothrombotic stroke model for characterizing TSP-1 expression after onset. (B) TSP-1 protein levels measured in isolated affected tissues from the stroke-induced hemisphere, contralateral hemisphere, and in serum. (C) TSP-1 protein levels in the stroke-affected hemisphere normalized to the corresponding contralateral hemisphere (n = 3). (D) Conjugation scheme for covalently binding TSP-1 and CLUVENA heparin nanoparticles to microgels and annealing of the microgels to form MAP scaffolds. (E) Cumulative TSP-1 release profiles rom TSP-1 nanoparticles (N = 3 and n = 3) and soluble TSP-1 (N = 3 and n = 3)-loaded MAP scaffolds.

amino acid residues with differing charge distributions. VEGF[20] contains strongly basic heparin-binding domains and is net positively charged at physiological pH, whereas TSP-1 is a larger protein with a near-neutral charge distribution, likely contributing to the more modest shift in zeta potential post-conjugation.[21–23] These results confirm successful nanoparticle functionalization and stability.

2.2. Heparin nanoparticles facilitate sustained release of TSP-1 in MAP scaffolds

After confirming successful conjugation of TSP-1 to heparin nanoparticles, we next sought to determine the appropriate dosing and delivery strategy for this therapeutic in a murine ischemic stroke model. While prior studies have demonstrated increased TSP-1 gene and protein expression post-stroke *via* qPCR and Western blotting, precise concentrations within brain tissue remain poorly defined.[12,24] Moreover, few studies have characterized TSP-1 expression over time in a photothrombotic (PT) model of ischemic stroke. Therefore, we performed an ELISA to directly quantify and verify whether similar patterns of TSP-1 protein expression existed in our PT stroke model.

A stroke was induced in the left hemisphere of the brain in the motor cortex area. Serum and brain tissue were collected from both hemispheres at 24 hours, 5 days, and 15 days post-induction (Fig. 2A). We observed a moderate but not statistically significant decrease in TSP-1 protein levels of 0.578 ng (±0.283) five days post-onset within the stroke affected hemisphere (Fig. 2B). However, the contralateral side showed no changes in TSP-1 protein levels on days 1, 5, and 15 after stroke, suggesting that changes in TSP-1 expression were more pronounced on the ipsilateral side (Fig. 2C).

Next, we assessed whether MAP scaffolds could be loaded with sufficient TSP-1 to exceed endogenous physiological levels, with the goal of achieving a supraphysiological dose capable of enhancing repair. Microgels, the hydrogel subunits of MAP scaffolds, were synthesized as previously described[5,14,25] from norbornene functionalized hyaluronic acid with a MMP cleavable cross linker and thiolated RGD peptide to encourage

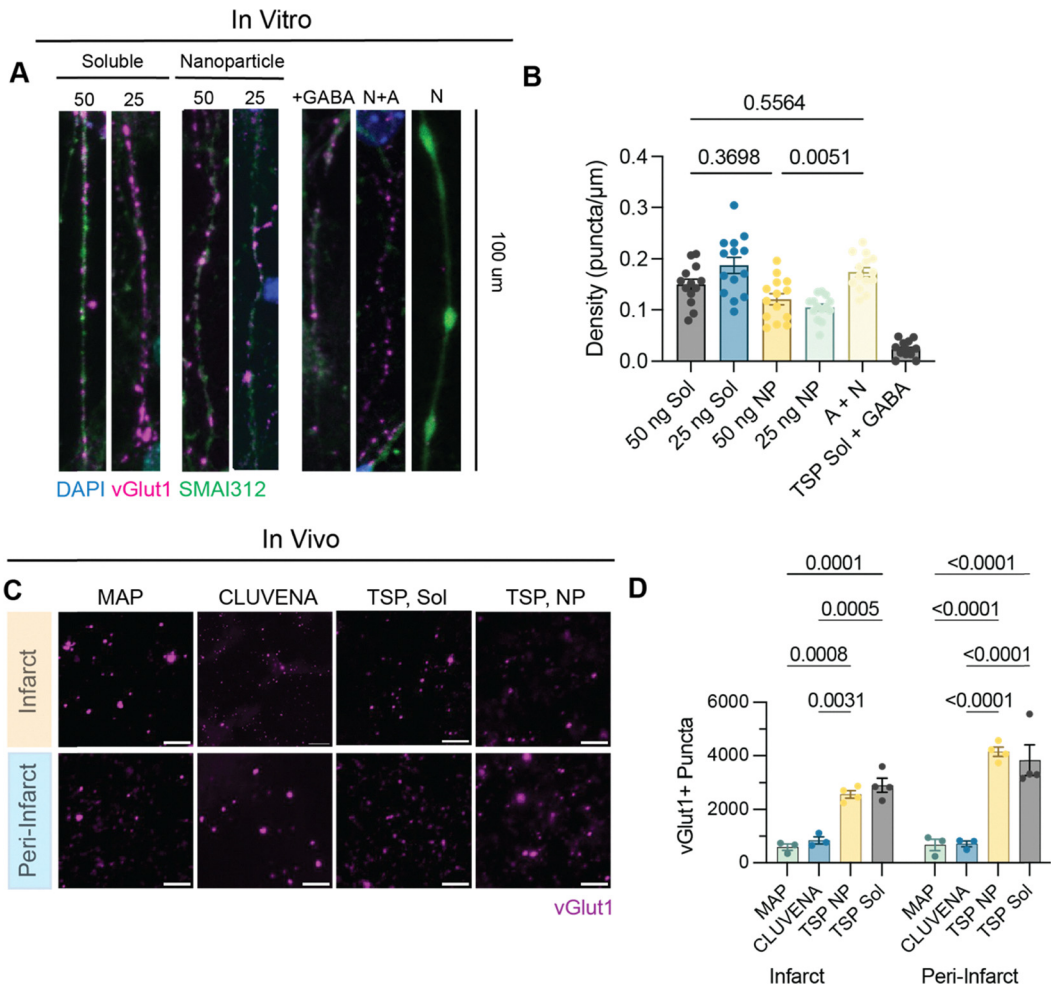

Fig. 3 Synapse formation in response to TSP-1 treatment. (A) 60× images of neurites taken from cortical neurons with pre-synaptic marker stain vGlut1 (magenta), SMI312 (green), and DAPI (blue). (B) Densities of synaptic puncta expressed on neurites. One way ANOVA with multiple comparisons (Sidak) was performed. n = 13–14 neurites. Unadjusted p-values are indicated on the graphs. (C) 60× images of the synapse marker (vGlut1) in magenta in the peri-infarct and infarct areas. (D) Densities of puncta were quantified in infarct and peri-infarct. Scale bars represent 5 µm. n = 3–4. Unadjusted p-values are indicated on the graphs.

cellular adhesion. TSP-1 nanoparticles and soluble TSP-1 were loaded into MAP scaffolds at a concentration of 200 ng of TSP-1 per 6 μL of MAP and subsequently annealed with HA-tetrazine (Fig. 2D). MAP scaffolds were incubated in PBS at 37 °C for 7 days to track TSP-1 release. Soluble TSP-1 exhibited an initial burst release of ~70 ng over the first 24 hours (Fig. 2E). In contrast, TSP-1 nanoparticles resulted in a modest burst release of on average 15 ng within the first 24 hours, before transitioning to a sustained release profile of <5 ng over the remaining 6 days. *In vitro*, TSP-1 Sol scaffolds were capable of releasing >50 ng of TSP-1 into the surrounding environment. In contrast, TSP-1 NP scaffolds retained over 50 ng within the biomaterial, maintaining a localized physiologically relevant concentration at the site of implantation. This distinction highlights the NP formulation's capacity to sustain therapeutic TSP-1 levels locally, while the soluble formulation enables broader distribution.

2.3. TSP-1 nanoparticles retain synaptogenic bioactivity both *in vitro* and *in vivo*

To determine if conjugated TSP-1 still retained its synaptogenic bioactivity post-conjugation, we performed a synapse formation assay *in vitro* by exposing cortical neurons to either 25 ng mL^{-1} or 50 ng mL^{-1} of TSP-1 protein in its soluble or nanoparticle form. Untreated cells and TSP-1 cotreatment with gabapentin, a known TSP-1 competitive inhibitor, served as negative controls.[9] Cells were fixed 48 hours post treatment and stained for the pre-synaptic marker vGlut1, as well as DAPI and for SMA312, a pan axonal cocktail. We found that there were no statistical differences in the vGlut1 puncta density between cells treated with 50 ng of either soluble or nanoparticle TSP-1, confirming that nanoparticle-bound TSP-1 retained its bioactivity (Fig. 3A and B).

Given these results, we evaluated whether this synaptogenic activity was retained when delivered *in vivo*, given that promoting synaptogenesis was a primary rationale for including TSP-1 in our treatment strategy. To assess this, we again stained for vGlut1 and evaluated the puncta density in and around the infarct site. We found that MAP + TSP-1 treatment in either soluble or nanoparticle forms increased synapse presence more than 2-fold in both the infarct and peri-infarct space, suggesting that active induction of synapse formation is possible *in vivo* with delivery of TSP-1 in either bound or soluble forms

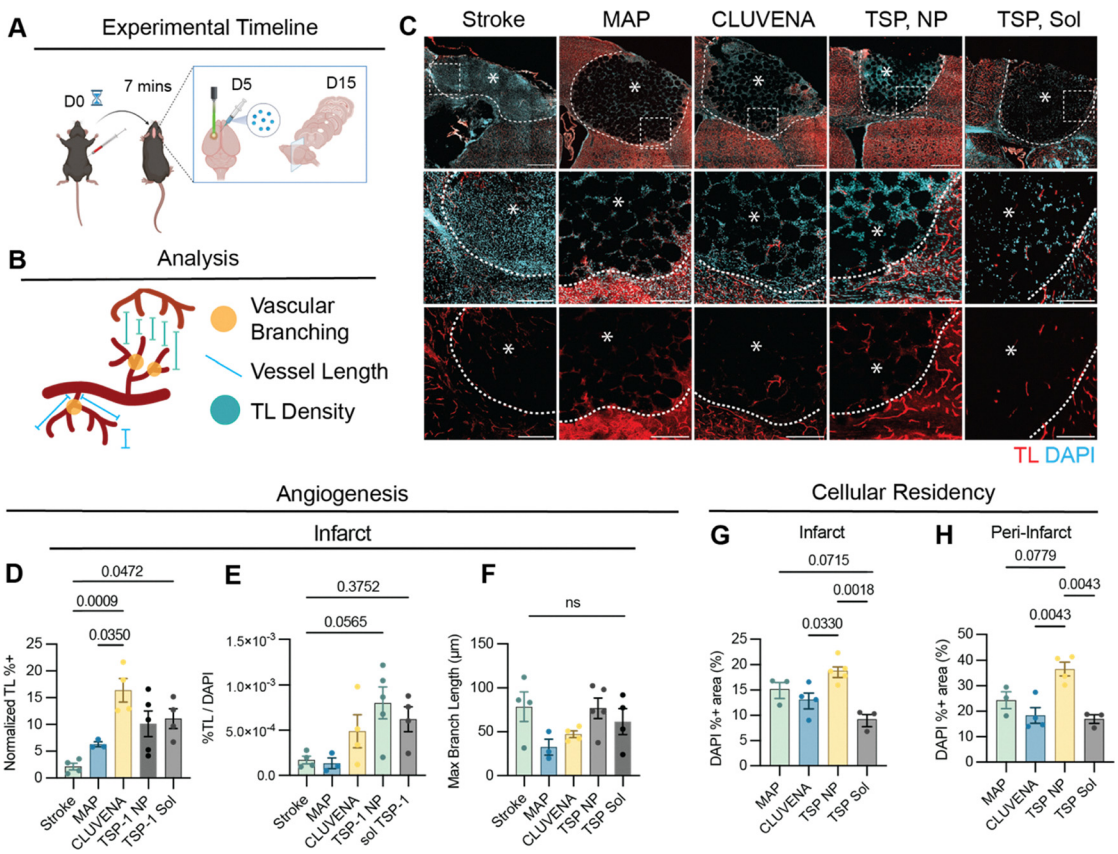

Fig. 4 Inclusion of TSP-1 does not hinder the angiogenic effect of CLUVENA + MAP 15 days after stroke. (A) Experimental timeline of PT stroke surgery. (B) Schematic outlining vascular characteristics analyzed. (C) Representative 20× large image scans of the infarct and surrounding tissue. Tissues were stained for perfusable vessels (Tomato Lectin) and nuclei (DAPI). Scale bars represent 500 μm. For magnified images, scale bar represents 200 μm. (D) Vasculature density measured in the infarct normalized to void space. (E) Vessel density normalized to DAPI count in the infarct. (F) Maximum branch length measured in the infarct. DAPI positive area measured in (G) the infarct and (H) the peri-infarct. For panels (D)–(H), averaged values were plotted with error bars representing the SEM. n = 3–4. Mixed effect analysis with Sidak *post hoc* analysis was performed. Unadjusted p-values are indicated on the graphs.

(Fig. 3C and D). Moreover, we observed similar levels of synapse formation in response to both bound and soluble TSP-1. This suggests that transient exposure to TSP-1 even without sustained local presence, may be sufficient to trigger synaptogenic programs in and around the stroke infarct.

2.4. Introduction of TSP-1 at the infarct site does not limit angiogenesis induced by CLUVENA

Our therapeutic approach aimed to leverage the angiogenic effects of clustered VEGF nanoparticles (CLUVENA) to work in concert with synapse formation induced by TSP-1 NPs. However, TSP-1 has also been reported to exert anti-angiogenic effects, which could directly counteract the VEGF-mediated pro-angiogenic activity of CLUVENA.[26] To evaluate whether our combinatorial approach had any anti-angiogenic effect, we delivered 6 μL MAP scaffolds annealed with HA-tetrazine and loaded with CLUVENA (containing 200 ng of VEGF), along with either TSP-1 Sol or TSP-1 NP containing 200 ng of TSP-1, directly into the infarct site *via* intracranial injection 5 days post-stroke (Fig. 4A). MAP scaffolds containing CLUVENA alone were included for comparison. Brains were harvested 15 days post-injection, a time point selected to coincide with the onset of the angiogenic response induced by MAP-CLUVENA treatment.

We observed that TSP-1 NPs did not inhibit the VEGF-mediated angiogenesis induced by CLUVENA within MAP scaffolds (Fig. 4D–F). All MAP treatments containing CLUVENA exhibited increased vascularization in the infarct compared to stroke only or mice treated with MAP alone (Fig. 4D). There were no statistical differences in the vascular density in the infarct area when comparing MAP + CLUVENA (16.39% ± 2.19) *versus* TSP-1 Sol (11.02% ± 2.60) or TSP-1 NPs (11.16% ± 2.31). When the vascular area was normalized to DAPI as an alternative measure, the TSP-1 nanoparticle group displayed the highest ratio of perfusable vasculature per cell (0.00062 ± 0.000137). This suggests a trend toward enhanced vascular density, though this difference did not reach statistical significance (Fig. 4E).

Additionally, there were no significant differences in the maximum branch length across groups, indicating comparable

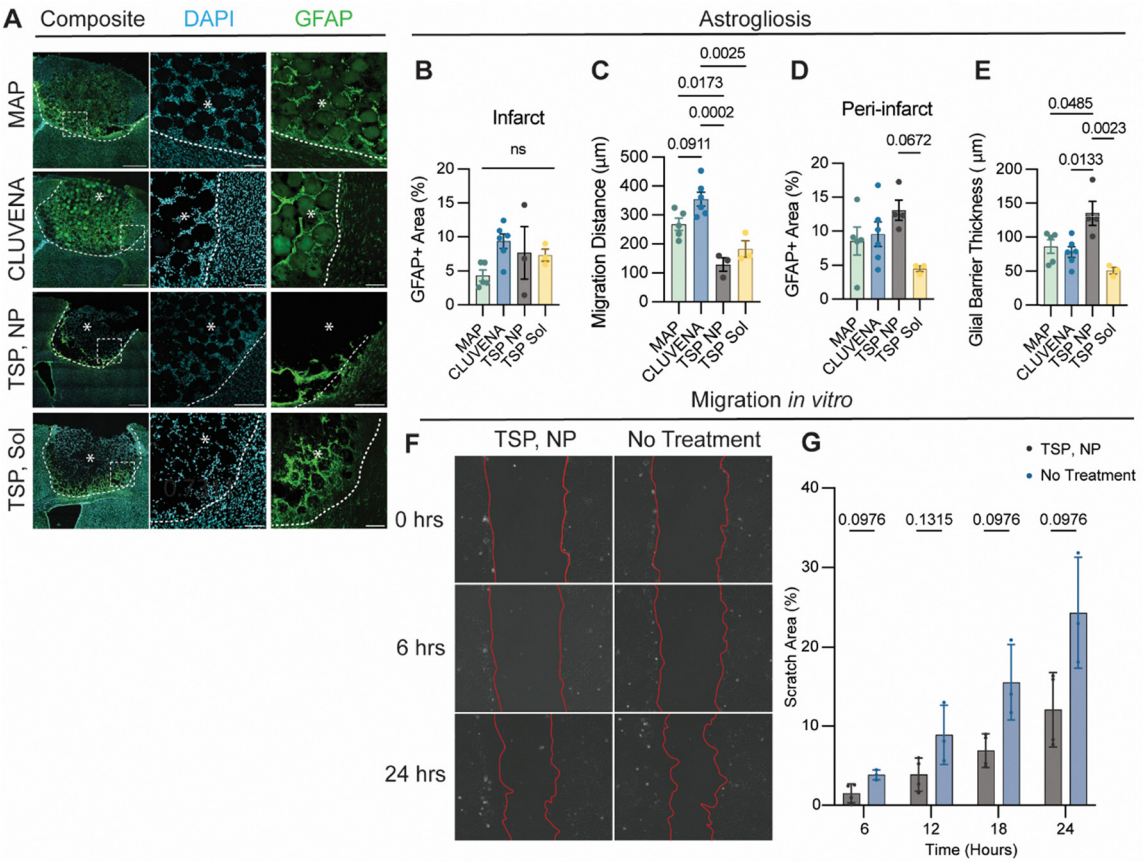

Fig. 5 TSP-1 NP MAP decreases astrocyte migration and increases astrogliosis. (A) Representative 20× immunofluorescence images stained for astrocytes (GFAP in green) and nuclei (DAPI in cyan) taken 15 days after stroke. Images were quantified for the GFAP percent positive area in the (B) infarct and (D) peri-infarct, (C) average migration distance into the infarct from the glial barrier, and (E) glial barrier thickness. Scale bars for the large image tile scan represent 500 μm. For magnified images, the scale bar represents 200 μm. n = 3–5. (F) Representative images from the astrocyte scratch migration assay where the (G) total scratch area recovered was measured 6, 12, 18, and 24 hours after wounding. (N = 3–4; n = 3). For panels (B)–(E), each data point is a biological replicate averaged over 2 coronal sections taken from the same animal and graphed. Error bars represent the SEM. For panel G, 3 FOVs for 3 wells of each condition were measured at times 0, 6, 12, 18, and 24 hours. Unadjusted p-values are indicated on the graphs and were measured using multiple unpaired t tests with Welch correction.

levels of vascular maturity in the infarct region (Fig. 4F). Following ischemic stroke, both VEGF-dependent and independent angiogenic programs are upregulated.[27,28] The sustained angiogenesis observed despite the inclusion of TSP-1 in the infarct site suggests that alternative non-VEGF pathways may compensate for or outweigh the anti-angiogenic effects of TSP-1.

TSP-1 delivery also appeared to influence the cellular dynamics within the MAP scaffold. An increase in void space between MAP microgels was observed in TSP-1 NP-treated mice, as indicated by a higher DAPI-positive area in both the infarct (18.82% ± 1.05) and peri-infarct (36.56% ± 2.70) areas compared to CLUVENA alone (infarct 13.12% ± 1.56; peri-infarct 18.38% ± 3.11) and even TSP-1 Sol (infarct 9.23% ± 1.20; peri-infarct 16.93% ± 1.73) (Fig. 4G and H). This phenomenon may be attributed to either increased cellular infiltration or enhanced degradation of the MAP scaffold. Interestingly, TSP-1 Sol exhibited the opposite trend, with decreased cellular residency in the infarct space.

2.5. Delivery of TSP-1 in MAP scaffolds results in reduced astrocyte infarct migration but does not change macrophage and microglia infiltration

Given the established roles of glial cells in supporting wound resolution and axonal regeneration, we next examined their response to our therapy post-stroke. As TSP-1 is frequently produced by glial barrier-forming astrocytes following stroke,[29] we investigated whether its increased presence in the infarct region could influence glial activation and immune cell dynamics following stroke by staining for GFAP positive astrocytes. While no significant differences were observed in the overall astrocyte density within the infarct core (Fig. 5B), astrocyte migration into the lesion was notably restricted in all groups treated with TSP-1 (Fig. 5C). Strikingly, mice receiving TSP-1 nanoparticles exhibited a significant increase in both the glial scar thickness (135.14 μm ± 24.9) and GFAP+ area (13.08% ± 2.10) in the peri-infarct compared to other treatment groups such as CLUVENA (glial barrier thickness, 78.19 μm ± 9.68; GFAP + area, 9.54% ± 2.21) and MAP alone (glial barrier thickness, 86.42 μm ± 13.20; GFAP + area, 8.52 ± 2.30) (Fig. 5D and E). Although treatment with TSP-1 Sol may have similarly decreased astrocytic migration in the infarct, we found that TSP-1 Sol dramatically decreased the glial barrier thickness compared to its NP counterpart (51.33 μm ± 8.07). These findings suggest that targeted delivery of TSP-1 to the infarct site may potentiate localized astrogliosis.

To further corroborate our *in vivo* observations in a more controlled environment, a scratch assay was conducted on monolayer astrocyte cultures to investigate the potential anti-migration effects of TSP-1 NPs on cellular migration. Astrocytes were scratched, treated with or without 100 ng TSP-1 NPs, and then monitored for 24 hours. We found that TSP-1 NP treatment lowered astrocyte migration into the open wound space over time, with the trend observed as early as 6 hours into the assay (Fig. 5F and G). Although TSP-1 upregulation has been linked to reactive astrocyte phenotypes, it has not previously been identified as a direct inducer of astrogliosis, indicating that its role in modulating astrocyte behavior may be context-dependent.

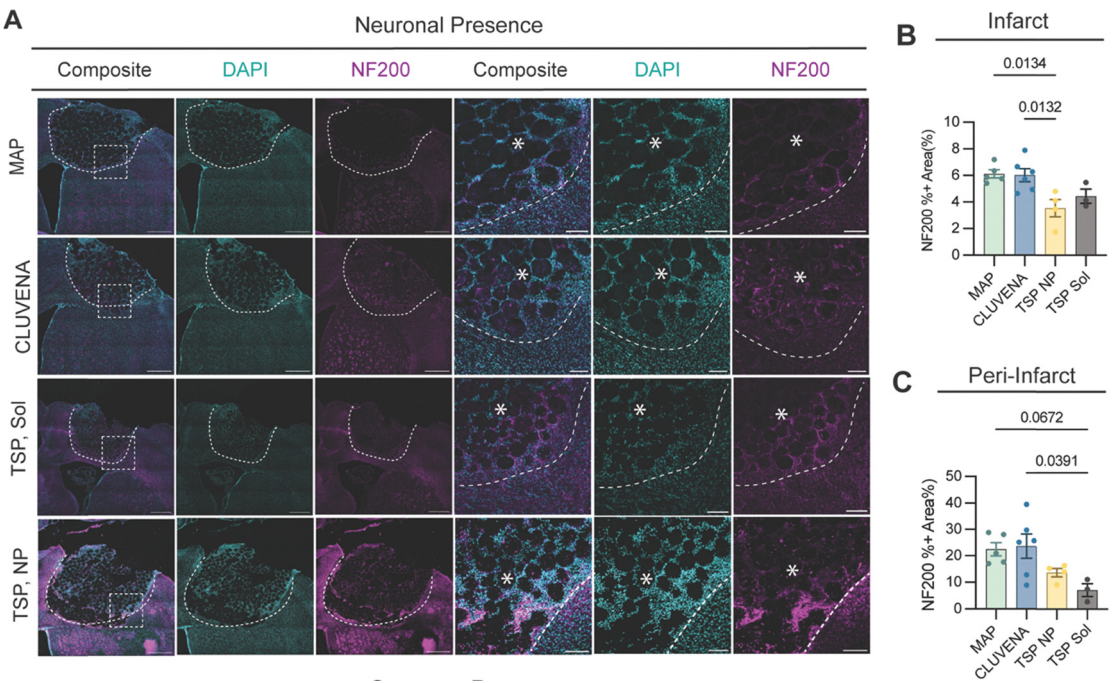

Fig. 6 TSP-1 nanoparticles hinder axonal sprouting 15 days after stroke. (A) 6 × 6 20× tile large image scan of stroke infarct with the neurons (NF200) in magenta and nuclei (DAPI) in cyan. Images were quantified for the NF200 percent positive area in the (B) infarct and (C) *peri* infarct. Scale bars represent 500 μm. For magnified images, the scale bar represents 200 μm. n = 3–5.

Infarct resolution after ischemic stroke is often mediated by both tissue resident and circulating immune cells and is crucial for promoting a neuroreparative environment.[30] Although TSP-1 has been reported to act as a chemoattractant for certain immune cell populations in other diseases,[31–33] this effect was not evident in our study. We observed no significant differences in macrophage or microglial densities within the infarct or peri-infarct regions across treatment groups (Fig. S1). The lack of heightened immune cell infiltration in our study suggests that localized TSP-1 delivery *via* nanoparticles may preclude undesirable pro-inflammatory responses.

2.6. TSP-1 nanoparticle treatment limits axonal sprouting

Increased axonal projections in and around the infarct site have been correlated with improved functional improvements in numerous stroke studies.[2,34] These newly sprouted axons act as the substrate for new neural connections to form as replacements for the engrams controlling behavior and cognition that are lost after ischemic stroke.[35] Prior work demonstrated that treatment with MAP + CLUVENA increased the neuronal marker NF200 expression in the infarct compared to MAP alone and stroke with no treatment.[5] NF200 presence was sustained into the chronic phase of healing suggesting that MAP + CLUVENA enabled a supportive environment with survival signals to sustain axonal presence long term, allowing them to form functional connections (not pruned/retracted). However, when CLUVENA was co-delivered with either TSP-1 NPs or TSP-1 Sol, we observed a reduction in axonal sprouting within both the infarct and the peri-infarct (Fig. 6A–C). Notably, TSP-1 Sol showed markedly less axonal sprouting in the peri-infarct region (7.14% ± 2.39) compared to both TSP-1 NPs (13.70% ± 1.59) and CLUVENA (23.61% ± 4.59). This finding was somewhat unexpected, as TSP-1 expression is often elevated in regions of active neurogenesis where synaptogenesis

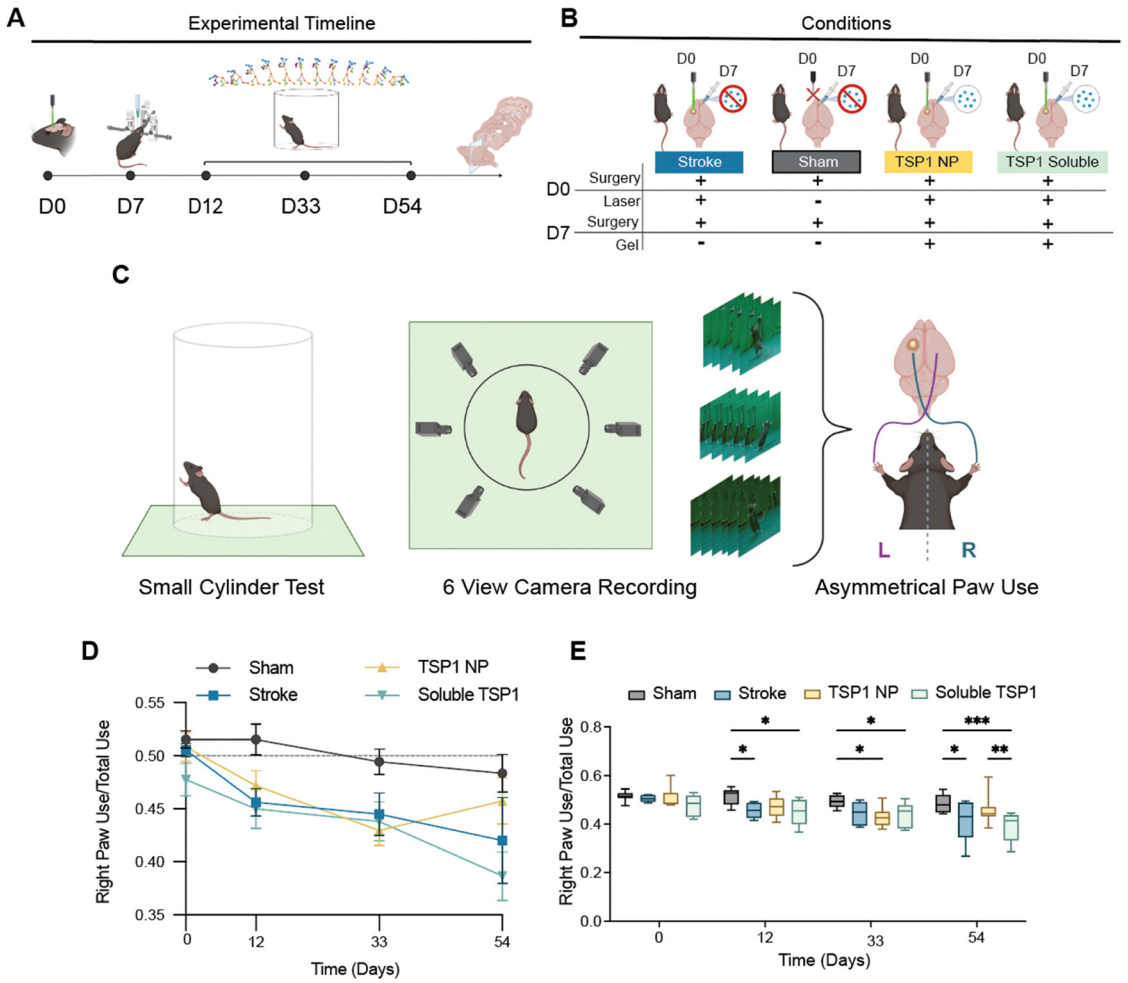

Fig. 7 (A) Experimental timeline for stroke induction and subsequent recordings at different time points. (B) Different experimental groups and the accompanying surgical manipulation. (C) Cylinder tests for measuring functional improvement. Animals were recorded from 6 different views simultaneously and 3-dimensional aligned neural network for computational ethology (DANNCE) was used to recapitulate behaviors in 3D space for asymmetrical limb use analysis. With stroke induced on the left motor cortex, the affected limb should be the right forepaw. Total affected (right) paw usage is represented by both a (D) line graph and (E) bar graph for sham, stroke, TSP NPs, and soluble TSP. Error bars for panels (D) and (E) represent S. E. M. with each point depicting a biological replicate (n = 4–6). For panel (E), mixed effects analysis was performed with a Sidak *post hoc* test comparing conditions across time. *$p < 0.05$, **$p < 0.01$, and ***$p < 0.001$.

and axonal sprouting can temporally and spatially overlap following injury.[13,24,36] We do suspect, however, that the previously observed thickening of the glial barrier in response to TSP-1 treatment (Fig. 5A–G) may have contributed to the observed reduction in NF200-positive axonal elongation into the infarct.

Given the limited axonal sprouting observed, we considered whether this might be in part due to reduced progenitor cell presence, which eventually could participate in neuronal differentiation and axonal sprouting. Prior literature has shown that knockout of TSP-1 impaired NPC proliferation and neuronal differentiation after ischemic stroke.[37] However, extrinsic modes of TSP-1 action have not yet been studied in this context. Therefore, we examined whether TSP-1 could promote progenitor cell proliferation in and around the infarct site. Additional staining with Sox2 showed no differences in progenitor cell presence across all groups (Fig. S2).

2.7. TSP-1 increases affected forepaw use after ischemic stroke

Ultimately, restoration of motor function is the primary treatment goal for ischemic stroke. Given that focal ischemia was induced in the left motor cortex, we anticipated contralateral motor deficits due to the lateralized nature of cortical motor control. Animals were subjected to the cylinder test to evaluate functional impairments and recovery as measured through vertical exploration and affected limb use. To perform high-resolution behavioral quantification, all cylinder test sessions were recorded through six synchronized camera angles. The resulting recordings were then processed using 3D Aligned Neural Network for Computational Ethology (DANNCE), a deep learning–based pose estimation pipeline optimized for multi-view reconstruction.[38] The approach enabled precise, three-dimensional tracking of forelimb kinematics, allowing for a temporally resolved analysis of limb use (Fig. 7C). Stroke, sham, and MAP delivered with CLUVENA and either soluble TSP-1 or TSP-1 nanoparticles were evaluated over 54 days (Fig. 7B). MAP was excluded since prior studies demonstrated that MAP alone did not elicit statistically significant functional improvement as measured with DANNCE.[39] Work performed by Erning *et al.* showed that MAP + CLUVENA significantly improved functional recovery after PT induced stroke.[5] By post-stroke day 54, animals treated with TSP-1–conjugated nanoparticles demonstrated a statistically significant increase in use of the affected contralateral forepaw during the cylinder test, indicating improvement in motor function compared to their soluble TSP treated counterparts. (Fig. 7D and E).

3. Conclusions

This study aimed to evaluate the feasibility and therapeutic potential of delivering soluble and nanoparticle forms of TSP-1 in the context of ischemic stroke. By leveraging the endogenous synaptogenic role of TSP-1, we aimed to restore neural circuitry in the infarct and peri-infarct regions. We observed promising trends in synapse formation, particularly in areas surrounding the stroke core, and several key findings offer new insights into the interplay between neurovascular, immune, and synaptic processes during recovery.

Compensatory revascularization of neural tissue is integral to functional recovery after stroke.[40,41] Angiogenesis reestablishes the vascular infrastructure necessary for nutrient delivery to affected but still viable neurons in the peri-infarct initially, and later to sprouting axons involved in neural rewiring.[42] Although vascularization within the infarct appeared consistent across all MAP-treated groups, the known anti-angiogenic effects of TSP-1 mediated through CD36 and CD47[43,44] were not evident at concentrations used. The local TSP-1 concentration ($\sim$200 ng) was well below the threshold (>0.5 μg mL^{-1}) required to inhibit angiogenesis *via* CD36 and CD47 signaling *in vitro*.[45,46] This indicates that localized delivery of TSP-1 does not compromise essential revascularization in the post-stroke microenvironment.

Besides its vascular effects, TSP-1 treatment led to a notable increase in the DAPI-positive area within the infarct, suggesting increased cellular residency in the implanted MAP scaffold. This observation is consistent with previous reports demonstrating that TSP-1 upregulates MMP-9 expression in endothelial cells,[47] positioning it as a key modulator of extracellular matrix remodeling. Our MAP scaffolds incorporate an MMP-cleavable sequence that is sensitive to both MMP-9 and MMP-2, allowing for scaffold degradation in the post-stroke brain environment where the MMPs are naturally upregulated. We hypothesize that the presence of TSP-1 may facilitate scaffold degradation, thereby creating additional space for cellular infiltration. However, the identity of the infiltrating cells remains unclear. Although TSP-1 has been reported to act as a chemoattractant for various immune cell types[48] and neural precursor cells,[37] we observed no significant differences in microglial or macrophage infiltration, nor in Sox2+ progenitor cell populations. These findings suggest that while endogenous TSP-1 may be necessary to support certain repair processes, exogenous supplementation does not further enhance the recruitment of these specific cell types following stroke.

Astrocytic responses also emerged as a key factor influencing recovery. Injury-associated pathways that trigger TSP-1 release, such as MAPK/ERK and STAT signaling, also reinforce the formation of a dense, reactive astrocytic barrier. While initially protective, this glial scar can later obstruct axonal regeneration and tissue reintegration. A central therapeutic goal moving forward will be to guide reactive astrocytes toward a more regenerative phenotype that supports, rather than hinders, circuit re-establishment.

Most importantly, we found that TSP-1 delivery promoted synapse formation but limited axonal elongation into the infarct. This observation highlights a key challenge in neural repair: the timing of synaptogenic *versus* axonogenic cues must be carefully balanced. By inducing synaptogenesis too early in the repair timeline, TSP-1 may inadvertently curtail axonal extension before sufficient target connectivity can be achieved.[49] By inducing synaptogenesis prematurely, TSP-1

may stabilize connections before sufficient axonal growth has occurred. To our knowledge, this is the first demonstration that a synaptogenic protein delivered *via* a biomaterial scaffold can directly modulate post-stroke connectivity.

Together, our results underscore the need for a more temporally precise modulation of synaptogenic signals in the post-stroke brain. Future iterations of this platform could include controlled-release strategies or environment-responsive delivery systems that delay the onset of TSP-1 activity until the structural groundwork for axonal regeneration has been laid. In doing so, we hope to more effectively balance the competing demands of axonal outgrowth and synaptic stabilization, ultimately guiding the brain toward more complete and functional recovery.

4. Experimental section/methods

4.1. Norbornene modification of heparin

Heparin modification with norbornene was performed as previously described.[15] 500 mg of heparin from porcine intestinal mucosa (Alfa Aesar, Cat. No A16198) and 735.5 mg of 4-(4,6-dimethoxy-1,3,5-triazin-2-yl)-4-methylmorpholinium chloride (DMTMM) (TCI Chemicals, Cat. No. 50-014-32155) were dissolved by stirring in 50 mM of MES buffer at pH 5.5 and allowed to react for 10 minutes at room temperature. Afterwards, 73.5 μL of 5-norbornene-2-methanamine (NMA) (TCI Chemicals, Cat. No. N0907) was added to the stirring mixture and allowed to react with the solution overnight at room temperature, protected from light. The next day, the modified polymer was dialyzed (molecular weight cutoff of 6–8 kDa) for 3 days against MilliQ water with water bath changes every 24 hours to remove the unreacted components. The final polymer product (Heparin-NB) was filtered through a 0.22 μM filter, then flash frozen, lyophilized, and kept at −20 °C until use. Norbornene modification was quantified by integrating the alkene proton resonances at δ6.00–6.30 ppm relative to the heparin *N*-acetyl methyl peak at δ2.00 ppm. Heparin-norbornene was confirmed by ^{1}H NMR with 71.6% norbornene modification. All equivalents were based on the moles of the heparin repeat unit.

4.2. Heparin nanoparticle synthesis & characterization

Heparin nanoparticle production was performed as previously described.[14,15] 100 mg of norbornene-modified heparin was dissolved in 500 μL of 0.3 M of HEPES buffer at pH 8.2 (Millipore Sigma, Cat. No. H3375) to make a 20% w/v solution. 0.27 mg of dithiothreitol (DTT) (Fisher Scientific, Cat. No. BP172-5) and 129 μL of 50 mM tris(2-carboxyethyl) phosphine (TCEP) (Millipore Sigma, Cat. No 580567) were added to the mixture. An organic phase consisting of 10 mL of hexane (Millipore Sigma, Cat. No. 320315), 123 μL Tween-80 (VWR, Cat. No. M126), and 383 μL of Span 80 (Millipore Sigma, Cat. No. 8.40123.01) was combined with the heparin-NB mixture. A horn sonicator was then used to sonicate the mixture to create the nanoparticles *via* reverse emulsion for one minute at 10% amplitude. Afterwards, 10 μL of TEMED was added and the mixture was again sonicated at the settings mentioned above. Then, 60 μL of 30% ammonium persulfate (APS) was added, and the solution was sonicated again using the same settings one final time. The mixture was allowed to react overnight stirring at 25 °C protected from light. To extract the nanoparticles, a liquid–liquid extract was used. To a separatory funnel, 10 mL of hexane, 10 mL of brine solution, and the heparin solution were added. The funnel was shaken, and layers separating the organic phase from the aqueous solution were allowed to form. The lower layer containing the brine and heparin nanoparticles were saved, and the hexane layer was discarded. A fresh 40 mL of hexane was once again combined with the extracted brine-heparin nanoparticle solution, and the process was repeated 5 times. Afterwards, the nanoparticles were dialyzed (molecular weight cut off of 100 kDa MW) against DI water with frequent bath changes for 2–3 days. Purified particles were emptied from the dialysis tubing, and kept at 4 °C, protected from light until use. The nanoparticles were filtered through a 0.22 μm filter before use after storage as particles can aggregate during storage. To characterize particle diameters, nanoparticles were loaded into a clean cuvette which was then loaded into an Anton Paar Litesizer DLS. Determination of the particle concentration was performed by measuring the weight before and after lyophilization of 1000 μL of the particle solution. The stability of all nanoparticle formulations was evaluated by monitoring changes in the particle size following dilution in an aqueous environment. The nanoparticles were diluted in MilliQ water at a concentration of 60 μg mL^{-1}. Samples were incubated at room temperature for the duration of the analysis, with the first reading taken immediately after dilution. Following incubation, the mean diameter was measured using dynamic light scattering (DLS) by intensity, and aggregation was assessed by comparing particle size distributions over time.

4.3. CryoEM

Quantifoil R 1.2/1.3 300 mesh copper grids were subjected to a 30 second plasma treatment using the easiGlow system (Ted Pella) prior to sample deposition. Cryo-sample preparation was carried out using a Vitrobot Mark IV (Thermo Fisher) under controlled conditions of 10 °C and 100% relative humidity. For nanoparticle samples, 3 μL of sample was applied to the carbon side of the grids. Blotting was performed for 3 seconds with a blotting force setting of −3, followed by rapid vitrification in liquid ethane. Data acquisition was performed using EPU software on a Tundra cryo-electron microscope (Thermo Fisher Scientific) operating at 100 kV.

4.4. TSP-1 and VEGF clustering on heparin nanoparticles

TSP-1 nanoparticles and VEGF nanoparticles (CLUVENA) were formulated by covalently tethering the protein to the surface of the heparin nanoparticles at a 20 : 1 mass ratio, as previously described.[5] In a low protein binding tube, either TSP-1 (Millipore Sigma, Cat. No. EM002) or VEGF (Biolegend, Cat. No. 583706) was added to a solution containing 10 mM LAP in 1× PBS at a ratio of 2 μg of protein per 0.1 μg of heparin

nanoparticles. The particles and protein were incubated on ice for 30 minutes, before exposure to UV (365 nm) at 20 mW cm^{-2} for 1 hour. For CLUVENA particles, the solution was transferred into 1% bovine serum albumin blocked 100 kDa Amicon filters (Millipore Sigma, Cat. No. UFC510024) and spun at 14 000 RPM for 10 minutes to remove unbound VEGF. The resulting particles were washed 4 times by adding 500 μL of 0.05% Tween-20 in PBS to the filter and centrifuging at 14 000 RPM for 10 minutes. The final particles were isolated by flipping the filter in a fresh tube, and centrifuging at 14 000 RPM for 15 minutes for CLUVENA. For TSP-1 nanoparticles, the reaction solution was instead placed in a 1 mL Spectra-Pore Float-A-Lyser (Repligen, Cat. No. G235036) with a MW cut off of 300 kDa. The nanoparticles were dialyzed against 200 mL of sterile water at 4 °C overnight. Particles were isolated from the dialysis device and further concentrated with a 1% BSA blocked 100 kDa Amicon filter to further concentrate the particles for experimental use. To measure binding efficacy, the dialysate was concentrated using 15 mL 100 kDa Amicon concentrators (Millipore Sigma, Cat No. UFC901000) and centrifuged at 5210 G for 30 minutes at a time until all dialysate was concentrated to ~300 μL. Concentrated unbound TSP-1 was then quantified using a TSP-1 ELISA as described below. Both nanoparticle formulations were kept at 4 °C until use within 7 days after synthesis.

4.5. TSP1 ELISA

TSP-1 binding efficacy, TSP-1 release, and TSP-1 tissue concentration were measured using a human TSP-1 DuoSet ELISA (R&D Systems, Cat. No. DY3074) following manufacturer's instructions. TSP-1 is highly conserved between humans and mice (~95%), allowing us to use the ELISA kit for detecting both mouse and human TSP-1. A standard curve of 100 ng mL^{-1} down to 1.56 ng mL^{-1} was used. All samples were used undiluted to be within the limit of detection.

4.6. Media preparation

Three different media formulations were used for the dissection and culture of neurons. A neuron pre-plating media was made consisting of a base of neurobasal media (Gibco, Cat. No. 21103049) with 1% penicillin–streptomycin (Gibco, Cat. No. 15140122), 0.3% L-glutamine (Gibco, Cat. No. 25030081), 0.6% sodium bicarbonate (Gibco, Cat. No. 25080084), and 5% normal horse serum (Gibco, Cat. No. 16050122). Dissection media consisted of a base of neurobasal media with 10% penicillin–streptomycin, 0.25% L-glutamine, 0.6% sodium bicarbonate, 10% normal horse serum, 10% glutamate (Millipore Sigma, Cat. No. 49621), and 2% B27. Neuronal culture media consisted of 10% penicillin–streptomycin, 0.25% L-glutamine, 0.6% sodium bicarbonate, and 2% B27. Formulations of media *sans* B27 was sterile filtered through a 0.22 μm filter prior to the addition of B27 and allowed to equilibrate in a 37 °C incubator with 5% CO_2 for at least 1 hour before use.

Astrocyte growth media (AGM) used for culture consisted of DMEM (Gibco, Cat. No. 11995073), 1% L-glutamate (Sigma-Aldrich, Cat. No. 49621), 1% of 10 000 U mL^{-1} of penicillin–streptomycin (Gibco, Cat. No. 15140122), and 10% normal horse serum (Gibco, Cat. No. 16050122).

4.7. Primary mouse cortical neuron isolation and culture

Neurons were isolated from cortical tissue as previously described.[50] For neuron isolation, a timed pregnant CD1 mouse (Charles River) was sacrificed *via* cervical dislocation. Afterwards, approximately 6–8 E15 embryos were isolated from the abdominal cavity and kept on ice in chilled 1% penicillin–streptomycin (Gibco, Cat. No. 15140122) in Hank's Balanced Salk Solution (Gibco, Cat. No. 1025092). After isolating the brain, cortices were dissected and digested for 10 minutes with 10 mL of 0.25% Trypsin/EDTA (Gibco, Cat. No. 25200056) with 500 μL of 40 000 U mL^{-1} DNase (Worthington Biochemical, Cat. No. LS002006) that had been equilibrated in a CO_2 incubator for a minimum of 30 minutes beforehand. Cortices were then transferred into a 50 mL conical tube containing 5 mL of pre-plating media with 250 μL of 40 000 U mL^{-1} DNAse and mechanically dissociated with a 1000 μL pipette until homogeneous. 30 seconds after dissociation, the supernatant was removed from the larger pieces of debris using a 1000 μL pipette and transferred into a new 50 mL conical tube. Cells were then pelleted by centrifugation at 1000 rpm for 5 minutes. After removal of the supernatant, the cells were resuspended in fresh neurobasal media and allowed to incubate in a TC-treated culture dish with pre-plating media at 37 °C for 40 minutes. This step allowed for the adhesion of contaminating cell types such as fibroblasts and astrocytes to attach to the culture dish. After the incubation, the supernatant solution containing neurons was filtered through a 100 μm filter, and once more pelleted before resuspension with 2 mL of day 1 media. To ensure accurate counting, a 1 : 50 dilution of the cell solution was created and counted manually using a hemocytometer. Cells were seeded (80 000 cells per well) onto PDL-coated coverslips (Neurovitro, Cat. No. GG-12-PDL) in a 24-well plate. 24 hours after seeding, the full volume of day 1 media was replaced with culture media. Afterwards, media were replaced every 5 days with culture media.

4.8. Astrocyte isolation and culture

P1 mouse pups were sacrificed by isoflurane inhalation. Cortices were dissected from the brain and digested with 10 mL of 0.25% Trypsin/EDTA (Gibco, Cat. No. 25200056) with 500 μL of 40 000 U mL^{-1} DNase (Worthington Biochemical, Cat. No. LS002006) that had been equilibrated in a CO_2 incubator for a minimum of 30 minutes beforehand. The cortices were then transferred into a 50 mL conical tube containing 5 mL of pre-plating media with 250 μL of 40 000 U mL^{-1} DNAse and mechanically dissociated with a 1000 μL pipette until homogeneous. 30 seconds after dissociation, the supernatant was removed from the larger pieces of debris using a 1000 μL pipette and transferred into a new 50 mL conical tube. Cells were then pelleted by centrifugation at 1000 rpm for 5 minutes. After removal of the supernatant, the cells were resuspended in fresh astrocyte growth media, filtered through a 100 μm filter, and plated onto PDL-coated 10 cm tissue culture treated Petri

dishes. 24 hours after initial plating, a full media change was performed. Afterwards, astrocytes were passaged every 6–7 days. Astrocytes up to passage number 3 were used in the experiments.

4.9. Synapse formation assay

The synapse formation assay was performed as previously described.[9] Day 10 neurons were used for synapse formation studies. Cells were exposed to 25 ng or 50 ng of TSP-1 in either nanoparticle or soluble form. Negative controls included co-incubation of TSP-1 nanoparticle or soluble forms with 32 μM of the known TSP-1 inhibitor Gabapentin (Millipore Sigma, Cat. No. G154). Positive controls included a co-culture of astrocytes with neurons at a 15 : 80 ratio of astrocytes to neurons starting at day 10. Cells were allowed to interact with treatments for 48 hours before fixation for further analysis.

4.10. Immunocytochemistry

48 hours post treatment, neurons were fixed with 4% paraformaldehyde (PFA) (Electron Microscopy Sciences, Cat. No. 15710-S) for 7 minutes at room temperature. Afterwards, they were washed with 1× TBS (Thermo Scientific, Cat. No. J60764.K7) three times to remove excess PFA. The cells were then incubated in blocking buffer consisting of 5% normal donkey serum (Millipore Sigma, Cat. No. S30), TBS, and a 0.2% Triton X-100 Surfact-Amps detergent solution for 2 hours at room temperature. Afterwards, a solution containing the primary antibodies of interest prepared in blocking buffer was introduced and allowed to incubate with the glass coverslips at 4 °C overnight. The next day, the primary antibody solution was removed, and the coverslips were washed three times with TBS with 0.2% Triton X-100 for 10 minutes on an orbital shaker. After these washes, a DAPI–secondary antibody solution prepared in blocking buffer was added and allowed to incubate with the neurons for a minimum of 2 hours protected from light. After incubation, samples were once more washed three times with TBS as described for 15 minutes. Glass coverslips containing the neurons were then mounted onto glass slides using Aqua/Poly Mounting (Polysciences, Cat. No. 18606-20) solution and allowed to dry at 4 °C for 2–3 days until imaging.

4.11. *In vitro* synapse imaging

Synapse formation was captured by confocal imaging after neuron fixation. All confocal images were taken on a Nikon Ti Eclipse scanning confocal microscope equipped with a C2 laser with a 60× oil immersion objective. A z-stack of at least 2 μm with a step size of 0.33 μm was taken for each region of interest. 2 regions of interest were taken from each coverslip to account for each technical replicate. The number of puncta was quantified for 100 μm of neurite length. Primary antibodies: 1 : 1000 vGlut1 (Synaptic Systems, Cat. No. 135 304), Homer (Synaptic System, Cat. No. 160 002), and SM1321 (Fisher Scientific, Cat. No. NC1239357). Secondary antibodies: 1 : 500 Alexa Fluor 488 (Mouse, Invitrogen, A32766), 1 : 500 Alexa Fluor 555 (Guinea Pig, Biotium, 2076), 1 : 500 Alexa Fluor 647 (Rabbit, Invitrogen, A-31573), and 1 : 500 DAPI (Sigma-Aldrich, D9542).

4.12. Modification of hyaluronic acid with either norbornene or tetrazine

Norbornene-modified hyaluronic acid and tetrazine-modified hyaluronic acid were synthesized as previously described.[25,51] Sodium hyaluronate also known as hyaluronic acid (HA) (~70 kDa, Contipro, Cat. No. 00-52-18) was modified with norbornene functional groups as previously described. A 200 mM MES (Millipore Sigma, Cat. No. M3671) buffer at pH 5.5 was first prepared. 1 g of Sodium hyaluronate was dissolved with 40 mL of 200 mM MES buffer *via* sonication. The carboxylic acids on the backbone of HA were then activated with 1092 mg of DMTMM for 20 minutes stirring at room temperature. Then, 2 molar equivalents of NMA and a 0.25 molar equivalent of the tetrazine amine HCl salt (Chem-Impex, Cat. No. 35098) were added to the solution and allowed to react for 24 hours at room temperature, protected from light. The next day, the modified HA was precipitated in chilled ethanol, centrifuged, and dried to remove the excess organic solvent. The modified polymers were then dialyzed (6–8 kDa molecular weight cut off) to remove the unreacted components, changing the dialysate every 24 hours against DI water across 3 days. After flash freezing in liquid nitrogen, the final product was lyophilized for long-term storage at 20 °C. Modification was characterized by proton NMR. Functionalization of norbornene-modified HA (HANB) was determined by ^{1}H-NMR shifts of pendant norbornenes in D_2O, δ6.33 and δ6.02 (vinyl protons and endo), and δ6.26 and δ6.23 ppm (vinyl protons and exo) compared to the HA methyl group at δ2.05 ppm. Functionalization of tetrazine-modified HA (HA-Tet) was determined by H NMR shifts of the pendant tetrazine groups at δ8.5 (2H) and δ7.7 (2H) (aromatic protons) compared to the HA methyl group at δ2.05 ppm.

4.13. Microgel production

HA-NB microgels were produced as previously described. Microgels were formed using a flow focusing microfluidic chip to create particles of the hydrogel. A hydrogel precursor solution consisted of 3.4% (w/v) hyaluronic acid modified with norbornene as described above, 1000 mM of RGD (RGDSPGERCG) (Genescript, custom synthesis), a di-thiol MMP peptide crosslinker (Ac-GCRDGPQGIWGQDRCG-NH2)-(Genescript, custom synthesis), di-sulfide reducer tris(2carboxyethyl) phosphine also known as TCEP (Millipore Sigma, Cat. No. 580567), and a photo initiator lithium phenyl(2,4,6-trimethylbenzoyl) phosphinate photo-initiator (LAP) (TCI America, Cat. No. L0290). The precursor solution was filtered through a 0.22 μm filter before loading into a 1 mL Luer lock syringe (BD, Cat. No. 309628) fitted with a blunt 23G needle. The oil solution consisted of 5% (v/v) Span-80 in heavy mineral oil. Droplets were crosslinked off chip with a UV light at 20 mW cm^{-2} (OmniCure LX500) and collected. The resulting microgels were washed first with a 5% pluronic solution to encourage mineral oil sequestration and removal. Particles were then spun down after washing with pluronic by centrifugation at 5250 G for 10 minutes. Additional washes with HEPES buffer followed to remove the remaining oil

and surfactant using the same centrifugation process. Particles were then stored in a HEPES solution with 1% pen/strep at 4 °C until use.

4.14. MAP scaffold generation and characterization

Microgels were isolated from storage solution through centrifugation at 14 000 G for 7 minutes. The supernatant was removed, and then microgels were spun down again at 14 000 G for 7 minutes to remove the remaining liquid. Microgels were then resuspended with either soluble TSP-1 (Millipore Sigma, Cat. No. ECM002-50UG) or TSP-1 nanoparticles using a positive displacement pipette to achieve a final concentration of 200 ng TSP-1/6 μL of gel. Then, HA-Tet was added to the microgel-TSP nanoparticle mixture through vigorous resuspension to achieve an annealing ratio (HA monomer/tetrazine) of 5.80.

4.15. TSP-1 MAP scaffold release study

For release studies, 12 μL of the MAP scaffold mixture was pipetted onto the bottom of a 24-well plate. Scaffolds were allowed to anneal at 37 °C for 1 hour. Then, 600 μL of 1× PBS was added to each well, and the plate was sealed with parafilm before incubation at 37 °C. 300 μL of sample buffer was withdrawn at each time point and replaced with 300 μL of fresh 1× PBS. Samples were then flash frozen in liquid nitrogen and stored at −20 °C before evaluation with a TSP-1 ELISA as described above.

4.16. Photothrombotic stroke

Induction of PT was performed as previously described and in accordance with the US National Institutes of Health and Animal Protection Guidelines and as approved by the Chancellor's Animal Research Committee. C57BL/6 male mice (Jackson Labs) of 8–12 weeks were positioned on a stereotaxic stage to immobilize the skull and intubate the animal under anesthesia. Rose Bengal (Millipore Sigma, Cat. No. 330000) was dosed at 10 mg mL^{-1} intraperitonially and allowed to circulate for 7 minutes. The skull was exposed, and a laser at 40 mw cm^{-2} was directed at the stereotaxic coordinate of 1.5 mm medial/lateral from the bregma. The laser was allowed to illuminate the brain through the skull for 13 minutes to induce the stroke infarct. The incision was then closed with Vetbond surgical glue (3 M, Cat. No. 70-0052-8246-5).

4.17. Stereotactic injection of MAP

Five days after ischemic stroke induction using the PT model, MAP scaffolds were injected into the infarct site. After positioning the anesthetized animal on the stereotaxic frame, the skull was exposed using the original incision created from the prior PT surgery. A burr hole was drilled at the same coordinates where the infarct was induced. A 10 μL glass syringe (Hamilton Company, Cat. No. 7635-01) with a 30-gauge needle (Hamilton Company, Cat. No. 7762-04) was loaded with 10 μL of the MAP scaffold and positioned at the skull opening. The needle was then lowered 0.750 mm into the infarct. 4.5 μL of the gel was then injected at a rate of 1 μL min^{-1} until the full volume was dispensed. The needle was allowed to sit for 3 minutes before removal to prevent accidental removal or displacement of the implanted hydrogel. The incision was then closed using Vetbond surgical glue, and animals were allowed to wake from anesthesia on a heating pad.

4.18. Tissue processing for ELISA

At terminal endpoints, animals were first anesthetized with isoflurane. A vena cava draw was then used to collect blood for serum isolation. After isolating the brain, a 4 mm biopsy punch was used to isolate the infarct and peri-infarct sites, as well as the correlating contralateral side. Tissue biopsies were then placed in low binding microcentrifuge tubes, flash frozen in liquid nitrogen, and kept at −80 °C until ready for processing. Brain tissue samples were then placed in a bead lysis tube with zirconium oxide beads (Next Advance, Cat. No. PINKR1) with 30× excess of T-PER tissue protein extraction reagent (Thermo Fisher Scientific, Cat. No. 78510). Tubes were then placed in a Bullet Blender (Next Advance, Troy, NY) and allowed to homogenize at speed 8 for 3 minutes at 4 °C. Samples were then further centrifuged at 10 000 G for 5 minutes at room temperature to remove debris. The supernatant from the sample was then isolated and stored at −80 °C until further analysis.

4.19. Tissue processing for histology

At terminal time points, animals were first anesthetized with isoflurane. Under anesthesia, a 50 μL retro-orbital injection of biotinylated Lycopersicon esculentum (tomato) Lectin (Vector Labs, Cat. No. B-1175-1) was administered and allowed to circulate for 10 minutes. Animals were then put under using isoflurane, and then transcardially perfused first with ∼10 mL of 1× PBS followed by 10 mL of chilled 4% (wt/vol) paraformaldehyde (PFA) (Electron Microscopy Sciences, Cat. No. 15710-S). Brains were then extracted and placed in 4% PFA for 4 hours at 4 °C. The brains were then rinsed with 1× PBS and then placed in 30% sucrose solution made with 1× PBS for a minimum of 24 hours at 4 °C. Brains were then cryosectioned into 30 μm sections collected on gelatin-coated glass slides. The slides were kept at −20 °C until staining.

4.20. Immunostaining

Slides were first acclimated to room temperature to remove residual moisture. They were then wash three times with 1× TBS with 0.2% Triton X-100 Surfact-Amps detergent solution (Thermo Fisher Scientific, Cat. No. 28314) (TBST) for 10 minutes. Afterwards, sections were placed in a blocking buffer consisting of 5% normal donkey serum in TBST for 2 hours. Slides were then incubated overnight at 4 °C with primary antibodies prepared in blocking buffer. After incubation, the slides were again washed three times for 10 minutes each with 1× TBS with Triton X-100. Secondary antibodies with DAPI (1 : 500) were then allowed to incubate with the tissues for 2 hours at room temperature shielded from light. Slides were washed again for a final time as previously described. Slides were then mounted using Aqua-Poly/Mount (Polysciences, Cat. No. 18606-20) and left to dry for 1–3 days at room temperature

protected from light. Primary antibodies: 1 : 250 NF200 (Millipore-Sigma, N4142), 1 : 250 PDGFRβ (R&D Systems, AF1042), 1 : 500 CD31 (BD, 557355), 1 : 1000 vGlut1 (Guinea Pig, AB5905), 1 : 250 Homer (Synaptic Systems, 160 002), 1 : 500 GFAP (Invitrogen, 13-0300), 1 : 250 TMEM119 (Synaptic Systems, 400 004), 1 : 250 IBA1 (Wako, 011-27991), and 1 : 500 Sox2 (Synaptic Systems, 347 003). Secondary antibodies: 1 : 500 Alexa Fluor 647 (Rb, Invitrogen, A31573), 1 : 500 Alexa Fluor 555 (Gt, Abcam, ab150130), 1 : 500 Alexa Fluor 488 (Streptavidin, Invitrogen, S11223), 1 : 500 CF 555 (Guinea Pig, Biotium, 2076), 1 : 500 Alexa Fluor 488 (Rt, Invitrogen, A21208), 1 : 500 Alexa Fluor 647 (Gt, Invitrogen, A21447), 1 : 500 Alexa Fluor 488 (Rb, Southern Biotech, 6442-30), 1 : 500 Alexa Fluor 647 (Streptavidin, Invitrogen, S32357), and 1 : 500 DAPI (Sigma-Aldrich, D9542).

4.21. Imaging and image analysis

Data points for each animal were reported as an average between two sections. Fiji/ImageJ was used to analyze the maximum intensity projections (MIPs) of 20× large fluorescence image scans taken with a Nikon Ti Eclipse scanning confocal microscope equipped with a C2 laser. ROIs were drawn around the infarct and peri-infarct (area surrounding the infarct 300 μm in all directions). Vessel diameters were determined using the straight line and measure tools with at least 10 different vessels measured and averaged per ROI. For vessel branching measurements (longest shortest path and the maximum branch length) images were despeckled, thresholded, and skeletonized. From the analyzed skeleton results, the maximum longest shortest path and maximum branch length were recorded for each ROI. The normalized signal area was found by dividing the signal PPA by the void space in the infarct. The void space was calculated by despeckling, Gaussian blurring (Sigma 8), thresholding, and finding the DAPI positive percent area in the infarct ROI.

4.22. Scratch assay

A monolayer of astrocytes was grown to ∼90% confluency on PDL-coated TC-treated 12-well plates as described above. A 200 μL pipette tip was used to create the scratch down the middle of the well against a straight edge. Wells were rinsed twice with warmed sterile PBS to remove debris before incubation in fresh astrocyte growth media with or without 100 ng of TSP-1 in the nanoparticle form. The plate was then placed in a Zeiss Axio Observer inverted microscope equipped with a Pecon XL S1 incubator system for live cell imaging. 3 fields of view capturing the scratch area and surrounding cells per well were taken every 30 minutes for 25 hours. During this time, the cells were maintained at 5% CO_2 and 37 °C. Frames taken at the 0-, 6-, 12-, 18-, and 24-hour time mark were then processed using the FIJI/ImageJ plugin Wound Healing Tool (RRID:SCR_025260).

4.23. Behavioral testing

Behavioral testing was performed as previously described.[5] The DANNCE arena consisted of 6 cameras mounted on a 30'' × 30'' breadboard. These cameras surrounded a stage on which a borosilicate glass cylinder (height 8'' diameter 4'') was placed in the center for recordings. The stage was further illuminated with 3 overhead LED lights (ikan Onyx, OYB240) to ensure adequate visibility for the cameras.

Prior to each session of animal recordings, the cameras underwent extrinsic and intrinsic calibration methods to aid with post processing triangulation of anatomical landmark translation into 3D Cartesian space from the video recordings. Intrinsic calibration of each camera was computed using AprilTags, a 2D fiducial marker array of QR codes, which were recorded for 15 seconds at 30 fps and processed using MATLAB code. Intrinsic calibration recordings were repeated until the mean pixel error was lower than 0.5 pixels and each recording had at least 150 frames. Afterwards, extrinsic calibration was performed by taking images of the calibration target with posts of known height and orientation. The quality of the extrinsic and intrinsic calibrations were assessed, and both calibrations were repeated if the mean pixel error was greater than 2.0 or the single camera pixel error was greater than 3.0.

After the mouse was placed in the glass cylinder, simultaneous recordings from all 6 cameras were taken of the subject's free movements for 5 minutes. After the recordings were finished, the animal was placed back in its housing unit, and the glass cylinder and stage were cleaned.

Video predictions of key anatomical points were performed by the DANNCE algorithm as described previously. DANNCE reconstructed a 3D volume from 6 camera views using calibrated camera parameters. On this 3D volumetric rendering, DANNCE estimated the 3D coordinates of anatomical key points in the real-world coordinate system. The key points of the forepaws were used to calculate the duration of the contact (paw use) with the cylinder during the rearing behavior, where a threshold of 2 mm was used to define contact. The usage of a forepaw is defined by the contact duration of that paw during rearing behavior. The total usage is the sum of both forepaw usage. This functioned as a measure for the asymmetrical behavior affected by stroke. The code and information to perform these key tasks can be found in the DANNCE GitHub repository.

4.24. Statistical analysis

For immunofluorescence image quantification of *in vivo* tissues, data were presented such that each point represents a single animal whereby values from 2 sections were averaged. Error bars represent the standard error of the mean (SEM). One way ANOVA was performed on the quantification of images with *post hoc* analysis (Sidak test). Animals were only excluded from analysis if tissue was damaged. For behavioral assessment, data were presented with error bars representing the standard error of the mean (SEM), where each animal was a biological replicate. Mixed effect analysis was performed to account for time and treatment factors. *Post hoc* test (Sidak) was performed to compare the treatment groups. Animals were excluded from analysis only if they prematurely passed or were

sacrificed early due to humane endpoint. Statistical analysis was performed using GraphPad Prism software (version 10.5.0).

Conflicts of interest

T. S. is a founder of Tempo Therapeutics that aims to commercialize MAP technology. T. W. D. is a co-founder and board member of dannce.ai, inc.

Data availability

Data for this article, including images and analysis files are available at https://doi.org/10.7924/r4k362427. The Github repository for the DANNCE scripts can be found here: https://github.com/Sooophy/dannce/tree/stroke_analysis/trace_protocol.

Supplementary information (SI) is available. See DOI: https://doi.org/10.1039/d5tb02179k.

Acknowledgements

The authors would like to thank Y. Ouyang, A. Jones, and C. Miksch for their helpful comments and feedback on earlier drafts of this work. We would like to thank K. Yang for his assistance with collecting the CryoEM images. The authors would like to acknowledge the following funding sources: the National Institutes of Health and the National Institute of Neurological Disorders and Stroke (R01NS079691) (T. S.), the National Institutes of Health (R01GM136972) (T. W. D.), and the National Institute on Drug Abuse (R34DA059512) (T. W. D.). This work was performed in part at the Duke University Shared Materials Instrumentation Facility (SMIF), a member of the North Carolina Research Triangle Nanotechnology Network (RTNN), which is supported by the National Science Foundation (award number ECCS-2025064) as part of the National Nanotechnology Coordinated Infrastructure (NNCI).

References

1 J. Bernhardt, K. S. Hayward, G. Kwakkel, N. S. Ward, S. L. Wolf and K. Borschmann, *et al.*, Agreed definitions and a shared vision for new standards in stroke recovery research: the stroke recovery and rehabilitation roundtable taskforce, *Neurorehabil. Neural repair*, 2017, **31**(9), 793–799.

2 S. T. Carmichael, B. Kathirvelu, C. A. Schweppe and E. H. Nie, Molecular, cellular and functional events in axonal sprouting after stroke, *Exp. Neurol.*, 2017, **287**, 384–394.

3 D. R. Griffin, W. M. Weaver, P. O. Scumpia, D. Di Carlo and T. Segura, Accelerated wound healing by injectable microporous gel scaffolds assembled from annealed building blocks, *Nat. Mater.*, 2015, **14**(7), 737–744.

4 L. R. Nih, E. Sideris, S. T. Carmichael and T. Segura, Injection of Microporous Annealing Particle (MAP) Hydrogels in the Stroke Cavity Reduces Gliosis and Inflammation and Promotes NPC Migration to the Lesion, *Adv. Mater.*, 2017, **29**(32), 1606471.

5 K. Erning, K. L. Wilson, C. S. Smith, L. Nguyen, N. I. Joesph, R. Irengo, *et al.*, Clustered VEGF Nanoparticles in Microporous Annealed Particle (MAP) Hydrogel Accelerates Functional Recovery and Brain Tissue Repair after Stroke, *bioRxiv*, preprint, 2025, DOI: 10.1101/2025.01.30.635733.

6 J. C. Adams and R. P. Tucker, The thrombospondin type 1 repeat (TSR) superfamily: Diverse proteins with related roles in neuronal development, *Developmental Dynamics: Dev Dyn*, 2000, p. 280–299.

7 W. Xu, S. Löwel and O. M. Schlüter, Silent Synapse-Based Mechanisms of Critical Period Plasticity, *Front. Cell. Neurosci.*, 2020, **14**, 213.

8 D. Vardalaki, K. Chung and M. T. Harnett, Filopodia are a structural substrate for silent synapses in adult neocortex, *Nature*, 2022, **612**(7939), 323–327.

9 Ç. Eroglu, N. J. Allen, M. W. Susman, N. A. O'Rourke, C. Y. Park and E. Özkan, *et al.*, Gabapentin Receptor α2δ-1 Is a Neuronal Thrombospondin Receptor Responsible for Excitatory CNS Synaptogenesis, *Cell*, 2009, **139**(2), 380–392.

10 K. S. Christopherson, E. M. Ullian, C. C. A. Stokes, C. E. Mullowney, J. W. Hell and A. Agah, *et al.*, Thrombospondins are astrocyte-secreted proteins that promote CNS synaptogenesis, *Cell*, 2005, **120**(3), 421–433.

11 J. Lawler, The functions of thrombospondin-1 and -2, *Curr. Opin. Cell Biol.*, 2000, 634–640.

12 J. Liauw, S. Hoang, M. Choi, C. Eroglu, M. Choi and G. H. Sun, *et al.*, Thrombospondins 1 and 2 are necessary for synaptic plasticity and functional recovery after stroke, *J. Cereb. Blood Flow Metab.*, 2008, **28**(10), 1722–1732.

13 X. Q. Dong, W. H. Yu, Q. Zhu, Z. Y. Cheng, Y. H. Chen and X. F. Lin, *et al.*, Changes in plasma thrombospondin-1 concentrations following acute intracerebral hemorrhage, *Clin. Chim. Acta*, 2015, **450**, 349–355.

14 K. L. Wilson, L. A. Onweller, N. I. Joseph, J. David-Bercholz, N. J. Darling and T. Segura, SDF-1 Bound Heparin Nanoparticles Recruit Progenitor Cells for Their Differentiation and Promotion of Angiogenesis After Stroke, *bioRxiv*, preprint, 2023, DOI: 10.1101/2023.07.05.547800.

15 L. R. Nih, S. Gojgini, S. T. Carmichael and T. Segura, Dual-function injectable angiogenic biomaterial for the repair of brain tissue following stroke, *Nat. Mater.*, 2018, **17**(7), 642–651.

16 N. A. Impellitteri, M. W. Toepke, S. K. Lan Levengood and W. L. Murphy, Specific VEGF sequestering and release using peptide-functionalized hydrogel microspheres, *Biomaterials*, 2012, **33**(12), 3475–3484.

17 C. Huang, Y. Liu, A. Beenken, L. Jiang, X. Gao and Z. Huang, *et al.*, A novel fibroblast growth factor-1 ligand with reduced heparin binding protects the heart against ischemia-reperfusion injury in the presence of heparin co-administration, *Cardiovasc. Res.*, 2017, **113**(13), 1585–1602.

18 M. H. Hettiaratchi, L. Krishnan, T. Rouse, C. Chou, T. C. McDevitt and R. E. Guldberg, Heparin-mediated

delivery of bone morphogenetic protein-2 improves spatial localization of bone regeneration, *Sci. Adv.*, 2020, **6**(1), eaay1240.
19 K. Tan, M. Duquette, J. H. Liu, R. Zhang, A. Joachimiak and J. H. Wang, *et al.*, The structures of the thrombospondin-1 N-terminal domain and its complex with a synthetic pentameric heparin, *Structure*, 2006, **14**(1), 33–42.
20 K. C. Scheiner, R. F. Maas-Bakker, M. J. van Steenbergen, S. P. Schwendeman, W. E. Hennink and R. J. Kok, Post-loading of proangiogenic growth factors in PLGA microspheres, *Eur. J. Pharm. Biopharm.*, 2021, **158**, 1–10.
21 W. J. Fairbrother, M. A. Champe, H. W. Christinger, B. A. Keyt and M. A. Starovasnik, Solution structure of the heparin-binding domain of vascular endothelial growth factor, *Structure*, 1998, **6**(5), 637–648.
22 W. S. Cho, F. Thielbeer, R. Duffin, E. M. Johansson, I. L. Megson and W. MacNee, *et al.*, Surface functionalization affects the zeta potential, coronal stability and membranolytic activity of polymeric nanoparticles, *Nanotoxicology*, 2014, **8**(2), 202–211.
23 J. W. Lawler, H. S. Slayter and J. E. Coligan, Isolation and characterization of a high molecular weight glycoprotein from human blood platelets, *J. Biol. Chem.*, 1978, **253**(23), 8609–8616.
24 T. N. Lin, G. M. Kim, J. J. Chen, W. M. Cheung, Y. Y. He and C. Y. Hsu, Differential regulation of thrombospondin-1 and thrombospondin-2 after focal cerebral ischemia/reperfusion, *Stroke*, 2003, **34**(1), 177–186.
25 A. R. Anderson, E. Nicklow and T. Segura, Particle fraction is a bioactive cue in granular scaffolds, *Acta Biomater.*, 2022, **150**, 111–127.
26 J. N. Sims and J. Lawler, Thrombospondin-1-Based Antiangiogenic Therapy, *J. Ocul. Pharmacol. Ther.*, 2015, **31**(7), 366.
27 T. Talwar and M. V. Srivastava, Role of vascular endothelial growth factor and other growth factors in post-stroke recovery, *Ann. Indian Acad. Neurol.*, 2014, **17**(1), 1–6.
28 L. Ruan, B. Wang, Q. ZhuGe and K. Jin, Coupling of neurogenesis and angiogenesis after ischemic stroke, *Brain Res.*, 2015, **1623**, 166–173.
29 G. E. Tyzack, S. Sitnikov, D. Barson, K. L. Adams-Carr, N. K. Lau and J. C. Kwok, *et al.*, Astrocyte response to motor neuron injury promotes structural synaptic plasticity via STAT3-regulated TSP-1 expression, *Nat. Commun.*, 2014, **5**, 4294.
30 E. Dzyubenko, D. Manrique-Castano, C. Kleinschnitz, A. Faissner and D. M. Hermann, Role of immune responses for extracellular matrix remodeling in the ischemic brain, *Ther. Adv. Neurol. Disord.*, 2018, **11**, 1756286418818092.
31 Z. Liu, S. Morgan, J. Ren, Q. Wang, D. S. Annis and D. F. Mosher, *et al.*, Thrombospondin-1 (TSP1) contributes to the development of vascular inflammation by regulating monocytic cell motility in mouse models of abdominal aortic aneurysm, *Circ. Res.*, 2015, **117**(2), 129–141.
32 G. Martin-Manso, S. Galli, L. A. Ridnour, M. Tsokos, D. A. Wink and D. D. Roberts, Thrombospondin 1 promotes tumor macrophage recruitment and enhances tumor cell cytotoxicity of differentiated U937 cells, *Cancer Res.*, 2008, **68**(17), 7090–7099.
33 E. V. Stein, T. W. Miller, K. Ivins-O'Keefe, S. Kaur and D. D. Roberts, Secreted Thrombospondin-1 Regulates Macrophage Interleukin-1beta Production and Activation through CD47, *Sci. Rep.*, 2016, **6**, 19684.
34 C. Kugler, C. Thielscher, B. A. Tambe, M. K. Schwarz, A. Halle and F. Bradke, *et al.*, Epothilones Improve Axonal Growth and Motor Outcomes after Stroke in the Adult Mammalian CNS, *Cell Rep. Med.*, 2020, **1**(9), 100159.
35 M. T. Joy and S. T. Carmichael, Encouraging an excitable brain state: mechanisms of brain repair in stroke, *Nat. Rev. Neurosci.*, 2020, **22**(1), 38–53.
36 T. Block, H. S. Isaksson, S. Acosta, M. Björck, D. Brodin and T. K. Nilsson, Altered mRNA expression due to acute mesenteric ischaemia in a porcine model, *Eur. J. Vasc. Endovasc. Surg.*, 2011, **41**(2), 281–287.
37 Z. Lu and J. Kipnis, Thrombospondin 1—a key astrocyte-derived neurogenic factor, *FASEB J.*, 2010, **24**(6), 1925.
38 T. W. Dunn, J. D. Marshall, K. S. Severson, D. E. Aldarondo, D. G. C. Hildebrand and S. N. Chettih, *et al.*, Geometric deep learning enables 3D kinematic profiling across species and environments, *Nat. Methods*, 2021, **18**(5), 564–573.
39 S. Xin, N. V. Phan, L. Zhang, S. T. Carmichael and T. Segura, Reactive astrocyte derived extracellular vesicles promote functional repair post stroke, *bioRxiv*, preprint, 2022, DOI: 10.1101/2022.09.06.506818.
40 H. Beck and K. H. Plate, Angiogenesis after cerebral ischemia, *Acta Neuropathologica*, Springer, 2009, p. 481–96.
41 J. Fang, Z. Wang and C. Y. Miao, Angiogenesis after ischemic stroke, *Acta Pharmacol. Sin.*, 2023, **44**(7), 1305–1321.
42 K. Arai, G. Jin, D. Navaratna and E. H. Lo, Brain angiogenesis in developmental and pathological processes: neurovascular injury and angiogenic recovery after stroke, *FEBS J.*, 2009, **276**(17), 4644–4652.
43 H. Chen, M. E. Herndon and J. Lawler, The cell biology of thrombospondin-1, *Matrix Biol.*, 2000, **19**, 597–614.
44 J. Lawler, Thrombospondin-1 as an endogenous inhibitor of angiogenesis and tumor growth, *J. Cell. Mol. Med.*, 2002, **6**(1), 1–12.
45 J. S. Isenberg, G. Martin-Manso, J. B. Maxhimer and D. D. Roberts, Regulation of nitric oxide signalling by thrombospondin 1: implications for anti-angiogenic therapies, *Nat. Rev. Cancer*, 2009, **9**(3), 182–194.
46 J. A. Rohrs, C. D. Sulistio and S. D. Finley, Predictive model of thrombospondin-1 and vascular endothelial growth factor in breast tumor tissue, *NPJ Syst. Biol. Appl.*, 2016, **2**, 16030.
47 X. Qian, T. N. Wang, V. L. Rothman, R. F. Nicosia and G. P. Tuszynski, Thrombospondin-1 modulates angiogenesis in vitro by up-regulation of matrix metalloproteinase-9 in endothelial cells, *Exp. Cell Res.*, 1997, **235**(2), 403–412.
48 S. Kaur and D. D. Roberts, Emerging functions of thrombospondin-1 in immunity, *Semin. Cell Dev. Biol.*, 2024, **155**(Pt B), 22–31.

49 P. P. Li and H. B. Peng, Regulation of axonal growth and neuromuscular junction formation by neuronal phosphatase and tensin homologue signaling, *Mol. Biol. Cell*, 2012, **23**(20), 4109–4117.
50 C. S. Smith, Z. Alvarez, R. Qiu, I. R. Sasselli, T. Clemons and J. A. Ortega, *et al.*, Enhanced Neuron Growth and Electrical Activity by a Supramolecular Netrin-1 Mimetic Nanofiber, *ACS Nano*, 2023, **17**(20), 19887–19902.
51 K. L. Wilson, S. C. L. Pérez, M. M. Naffaa, S. H. Kelly and T. Segura, Stoichiometric Post-Modification of Hydrogel Microparticles Dictates Neural Stem Cell Fate in Microporous Annealed Particle Scaffolds, *Adv. Mater.*, 2022, **34**(33), 2201921.